# GENERATION OF MULTI-MODAL LAMB WAVES FOR THE INSPECTION OF THIN AERONAUTICAL STRUCTURES

Andreea-Denisa GRIGUȚĂ[1], Mihai Valentin PREDOI[2]*

*Many researchers presented various aspects concerning the Lamb waves, from methods to obtain the dispersion curves, to the assessment of discontinuities geometry, by numerical and experimental methods. Due to their capacity to travel along the planar structures, the Lamb waves can inspect large structures, from a single point of generation-reception of ultrasonic signals, based on scattering of incident waves by small defects. The scattering phenomenon is more complex as the frequency increases and more Lamb modes can propagate. Most authors have chosen a single incident mode for this reason, which is a limiting factor in many cases. The present paper is investigating a normal incidence piston-like excitation of multi-modes Lamb waves. The advantage is that the transducer energy is entirely transmitted to the structure. The trade-off is represented by the requirement to compute the incident energy associated with each of the Lamb modes from the incident wave.*

**Keywords**: Lamb waves, piston excitation, multimode propagation.

## 1. Introduction

Lamb waves, named after their discoverer [1], are nowadays presented in most ultrasonic textbooks e.g. [2], [3] and are used in technical applications, especially in non-destructive evaluation of planar structures, due to their long-range propagation in comparison to bulk waves. The classical Lamb waves propagate along homogeneous isotropic plates and are made of one or several Lamb modes, belonging to one of the two classes of modes: symmetric and antisymmetric (skew-symmetric as some authors prefer). A dedicated monography was published in 1967 by Viktorov [4].

The amplitude of each such mode depends on the generation method and on the scattering phenomena occurring during the propagation along the plate. Scattering is a process of splitting the incident modes into all possible propagating modes, in such a manner that the boundary conditions over the discontinuity are fully met. Determining the modal amplitudes from a scattering process relies on

[1] Stud., Faculty of Aerospace Engineering, University POLITEHNICA of Bucharest, Romania, e-mail: griguta_andreea_denisa@yahoo.com
[2] Prof., Deptartment of Mechanics, Fac. I.S.B, University POLITEHNICA of Bucharest, Romania, e-mail: mihai.predoi@upb.ro (* corresponding author)

modal orthogonality proven by Fraser [5] and in a another form by Murphy and Chin-Bing [6].

One of the first investigated discontinuity is represented by the plate end considered to be perpendicular on the free surfaces of the plate. Torvik [7] used the reciprocity relation to decompose the incident Lamb mode into a series of Lamb modes reflected from a free normal end of an elastic plate. Gregory and Gladwell [8] used an orthogonality formula for the this reflection problem. Galan and R. Abascal [9], [10] used a hybrid finite elements- boundary elements method to solve the reflection problem, using an original method to compute the dispersion curves. Predoi and Rousseau determined the symmetric and antisymmetric Lamb modes amplitudes, scattered from a free edge of a plate for a wide range of frequencies [11], using a series of modes including non-propagating modes. These modes were presented in detail by Predoi in ref. [12]. An important experimental validation, emphasizing the so-called "edge mode" was investigated by Le Clezio et al. [13].

The present work is organized as follows. The theoretical aspects related to the dispersion curves are presented in section 2. The scattering phenomenon at the plate incidence end is presented in section 3, using an analytical method based on orthogonality theorems [5], [6], providing the incident energy of each mode, for a given plate at a wide range of frequencies. A qualitative experimental validation is proving the modal decomposition validity over a relatively large frequency range.

## 2. Theoretical aspects

### 2.1 Dispersion curves

In a homogeneous isotropic plate occupying the domain: $\{(x,z);\, x\in[0,\infty),\ z\in[-h/2,\, h/2]\}$ (Fig. 1) the elasticity equations are fulfilled by two potentials. One is the scalar potential $\varphi(x,z,t)$ satisfying the wave equation for the longitudinal (compressional) waves $c_L^2\Delta\varphi=\ddot{\varphi}$ and the other is a vector potential $\bar{\psi}(x,z,t)$ describing the transversal (shear) waves $c_T^2\bar{\Delta}\bar{\psi}=\ddot{\psi}$ with possible horizontal (SH) or vertical (SV) polarizations relative to the indicated axes. A supplementary "gauge" condition is imposed to the third scalar component, so that finally in an elastic solid there are three scalar functions describing the possible elastic waves.

The two bulk velocities are related to the elasticity constants (Lamé constants λ, μ) and mass density ρ, by the classical formulas:

$$c_L=\sqrt{\frac{\lambda+2\mu}{\rho}};\quad c_T=\sqrt{\frac{\mu}{\rho}}\ . \tag{1}$$

In the particular case of the Lamb waves, the displacements field has only two components: *u(x,y,t)* along the Ox axis and *w(x,y,t)* along the Oz axis.

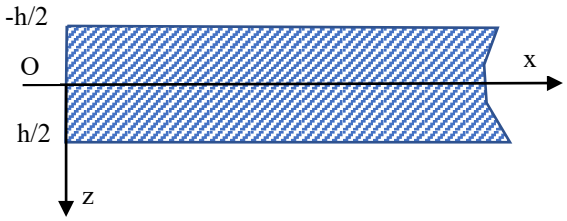


Fig. 1 Geometry of the semi-infinite plate

The following harmonic forms of the scalar potential and the relevant component of the vector potential are written as [4], [2]:

$$\begin{aligned} \varphi &= S_L \cos\left(k_{Lz} z\right) \exp\left[i\left(k_x x - \omega t\right)\right] \\ \Psi &= S_T \sin\left(k_{Tz} z\right) \exp\left[i\left(k_x x - \omega t\right)\right] \end{aligned}, \tag{2}$$

which allow writing the symmetrical displacements about the Oxy plane:

$$\begin{aligned} u &= \frac{\partial \varphi}{\partial x} - \frac{\partial \Psi}{\partial z} = \left[iS_L k_x \cos\left(k_{Lz} z\right) - S_T k_{Tz} \cos\left(k_{Tz} z\right)\right] \exp\left[i\left(k_x x - \omega t\right)\right] \\ w &= \frac{\partial \varphi}{\partial z} + \frac{\partial \Psi}{\partial x} = \left[-S_L k_{Lz} \sin\left(k_{Lz} z\right) + iS_T k_x \sin\left(k_{Tz} z\right)\right] \exp\left[i\left(k_x x - \omega t\right)\right] \end{aligned}. \tag{3}$$

The following notations have been used:

$$\begin{aligned} &\omega = 2\pi f;\ \ k_x = \frac{\omega}{c};\ k_T = \frac{\omega}{c_T};\ k_L = \frac{\omega}{c_L}; \\ &k_{Tz} = \sqrt{k_T^2 - k_x^2};\ k_{Lz} = \sqrt{k_L^2 - k_x^2} \end{aligned} \tag{4}$$

in which $f$ is the frequency (Hz) and $c$ is the phase velocity of a Lamb mode, whereas $k_x$ denotes the Ox component of the wavenumber, $S_L$ and $S_T$ represent the complex valued amplitudes, which are corelated for a given Lamb mode, after solving the dispersion equation. For small displacements, the relevant strain components in the elastic material are:

$$\varepsilon_x = \frac{\partial u}{\partial x};\quad \varepsilon_z = \frac{\partial w}{\partial z};\quad \gamma_{zx} = \frac{\partial u}{\partial z} + \frac{\partial w}{\partial x}. \tag{5}$$

The associated stress components can be developed as:

$$\sigma_{xx}=(\lambda+2\mu)\frac{\partial u}{\partial x};\ \sigma_{zz}=(\lambda+2\mu)\frac{\partial w}{\partial z};\ \sigma_{xz}=\mu\left(\frac{\partial u}{\partial z}+\frac{\partial w}{\partial x}\right) \tag{6}$$

Injecting the displacements expressions (3) in the stress formulas (6), one can deduce the dispersion equation for symmetric Lamb modes [1], [4], by enforcing cancellation of stresses: normal $\sigma_{zz}(\pm h/2)=0$ and shear $\sigma_{xz}(\pm h/2)=0$:

$$C_s(k_x,\omega)=4k_x^2k_{Lz}k_{Tz}\tan(k_{Lz}h)+\left(2k_x^2-k_T^2\right)^2\tan(k_{Tz}h)=0\ . \tag{7}$$

In a similar manner, antisymmetric modes are obtained from the potential formulas:

$$\varphi=A_L\sin(k_{Lz}z)\exp\left[i(k_xx-\omega t)\right];\ \Psi=A_T\cos(k_{Tz}z)\exp\left[i(k_xx-\omega t)\right] \tag{8}$$

as:

$$C_a(k_x,\omega)=4k_x^2k_{Lz}k_{Tz}\tan(k_{Tz}h)+\left(2k_x^2-k_T^2\right)^2\tan(k_{Lz}h)=0\ . \tag{9}$$

The authors developed a numerical method for solving these dispersion equations, based on the residuals theorem [14]. More detail concerning this numerical algorithm can be found in refs. [11] and [12]. For a chosen frequency, the full range of real, imaginary and complex roots are obtained, forming continuous curves for each mode, denoted $S_0$, $S_1$, $S_2$, $S_3$, …, $A_1$, $A_2$, etc. The real nondimensional wavenumbers ($k_xh$) indicate propagating modes, which exist for non-dimensional frequency ($\omega h/c_T$), marked by black dots on Fig. 2. Blue dots indicate purely imaginary wavenumbers and green dots indicate complex conjugate wavenumbers. The modes $S_1$, $S_2$, … are propagating only above the so-called cut-off frequencies, visible in this figure.

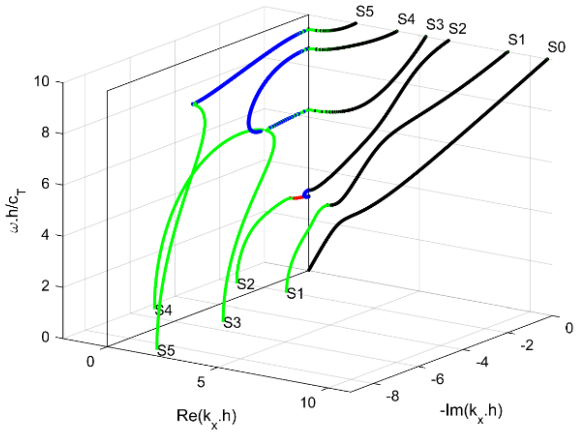


Fig. 2 Dispersion curves for symmetric modes

These last two types of wavenumbers represent non-propagating (or evanescent) modes, which are useful only in expressing boundary conditions, since these modes do not propagate far in the plate. For propagating modes only, on Fig. 3 are shown the wavenumbers vs. frequency in both nondimensional ($k_x h$, $\Omega = \omega h / c_T = k_T h$) and physical quantities ($k_x$, usual frequency $f$ [kHz] ) for a 3mm thick aluminum plate.

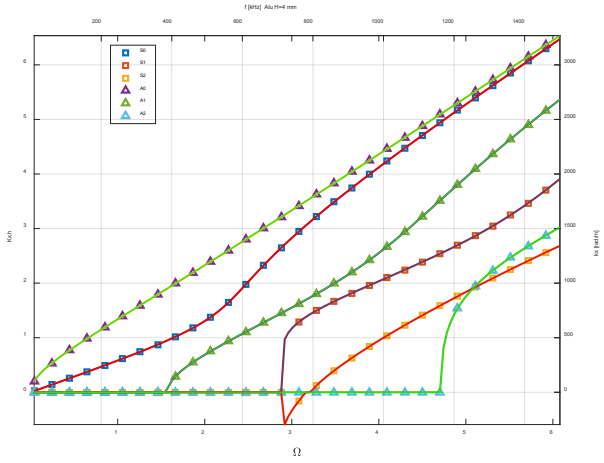


Fig. 3 Dispersion curves for Lamb modes in an aluminum plate

The antisymmetric modes are included in this figure, up to $A_2$. Negative wavenumbers indicate a particular frequency domain in which the phase and group velocities have opposite signs.

## 2.2 Modal decomposition

It has been proven by Murphy and Chin-Bing [5] and by Brazier-Smith and Scott [6] that any stress or displacements field of a propagating ultrasonic wave in a plate, can be decomposed in an infinite series of propagating and evanescent modes, coexisting at that particular frequency, using their property of energy flux reciprocity or modal orthogonality. The modal amplitudes are obtained using this procedure, using the dispersion curves, mentioned in the previous section.

If the ultrasonic wave is a chirp or any arbitrary ultrasonic signal, the method can be applied for each individual frequency of the spectrum, obtained by applying a Fourier series (FFT) decomposition of the temporal signal.

Our analysis is focused on symmetric modes, provided that the plate has a perpendicular edge where the ultrasonic transducer will be placed. Due to the geometric symmetry of the problem, it can be easily proven that only symmetric

Lamb modes can be generated by the longitudinally oscillating perpendicular edge. The symmetric displacements (3) will be written in a more compact form, for a particular symmetric Lamb mode of order n =0, 1, 2, … :

$$\begin{bmatrix} u(x,z,t) \\ w(x,z,t) \end{bmatrix}_n = S_n \begin{bmatrix} U_{xn}(z) \\ U_{zn}(z) \end{bmatrix} \exp\left[ i\left(k_{xn}x - \omega t\right)\right] \tag{10}$$

in which $S_n$ is an arbitrary constant representing the (complex) amplitude of mode $n$. The other constant from (3) is no longer independent after solving the dispersion equation, being provided by their ratio:

$$B_{Sn}\left(\omega, c_L, c_T\right) = \frac{2k_{xn}k_{Lzn}\sin\left(k_{Lzn}h\right)}{\left(k_{Tzn}^2 - k_{xn}^2\right)\sin\left(k_{Tzn}h\right)}. \tag{11}$$

Consequently, the displacement field of any particular symmetric Lamb mode can be written, leaving aside the harmonic factor $\exp\left[ i\left(k_{xn}x - \omega t\right)\right]$ as [11]:

$$\begin{bmatrix} U_x \\ U_z \end{bmatrix}_n = \begin{bmatrix} ik_{xn}c_{Lzn} - iB_{Sn}k_{Tzn}c_{Tzn} \\ -k_{Lzn}s_{Lzn} - B_{Sn}k_{xn}s_{Tzn} \end{bmatrix}. \tag{12}$$

The axial and shear stress functions along the normal direction onto the free plate surfaces are:

$$\begin{bmatrix} S_{xx} \\ S_{zx} \end{bmatrix} = \mu \begin{bmatrix} -\left(k_T^2 - 2k_{Lz}^2\right)c_{Lzn} + 2B_s k_x k_{Tz} c_{Tzn} \\ -2ik_{Lz}k_x s_{Lzn} - B_s\left(k_{Tz}^2 - 2k_x^2\right)s_{Tzn} \end{bmatrix} \tag{13}$$

The following notations have been used :

$c_{Lzn} = \cos\left(k_{Lzn}z\right)$; $s_{Lzn} = \sin\left(k_{Lzn}z\right)$; $c_{Tzn} = \cos\left(k_{Tzn}z\right)$; $s_{Tzn} = \sin\left(k_{Tzn}z\right)$.

Finally, any displacement field at a given frequency $f$ at $x=0$, can be expressed as a sum of Lamb modes:

$$\begin{bmatrix} \mathrm{U}(\mathrm{z}) \\ \mathrm{W}(\mathrm{z}) \end{bmatrix} = \sum_{n=0}^{\infty} S_n \begin{bmatrix} U_x(z) \\ U_z(z) \end{bmatrix}_n. \tag{14}$$

### 3. Modes generated by a piston transducer

An ultrasonic transducer has a planar surface oscillating at high frequency, usually being excited by an electric pulse, and generating an ultrasonic chirp. A chirp can be decomposed in harmonic signals of amplitudes $A_m$ and frequencies $f_m$ obtained from an harmonic analysis (FFT). Consequently, our investigation can be

continued at a frequency $f_m$ and an arbitrary amplitude $A_m$ . In a practical case, the obtained results can be summed, according to the superposition principle applied for linear phenomena. An important hypothesis has to be introduced at this stage: the transducer which is pressed against the plate edge at *x=0*, produces only longitudinal displacements and stresses and no tangential displacements, nor shear stresses:

$$\begin{bmatrix} \mathrm{U}(\mathrm{z}) \\ \mathrm{W}(\mathrm{z}) \end{bmatrix} = \begin{bmatrix} U_0 \\ 0 \end{bmatrix}. \tag{15}$$

Consequently, in this case the boundary conditions at x=0 are written as a sum of modal displacements, marked by index *n*:

$$\sum_{n=0}^{\infty} S_n \begin{bmatrix} U_x(z) \\ U_z(z) \end{bmatrix}_n = \begin{bmatrix} U_0 \\ 0 \end{bmatrix}. \tag{16}$$

In order to determine the $S_n$ modal amplitudes for the modes of interest, the following reciprocity relation will be used [7], with $T_{xx}$ and $T_{zx}$ being components of the stress field to be decomposed into Lamb modes. A bar above a quantity represents the complex conjugate of the respective quantity:

$$\int_{-h}^{h} \left( U_x^{(m)} \overline{T}_{xx} + U_z^{(m)} \overline{T}_{zx} \right) dz = \sum_{n=0}^{\infty} S_n \left[ \int_{-h}^{h} \left( U_x^{(m)} \overline{S}_{xx}^{(n)} + U_z^{(m)} \overline{S}_{zx}^{(n)} \right) dz \right]. \tag{17}$$

In the present work, the left side of this equation is simpler:

$$P \int_{-h}^{h} U_x^{(m)} dz = \sum_{n=0}^{\infty} S_n \left[ \int_{-h}^{h} \left( U_x^{(m)} \overline{S}_{xx}^{(n)} + U_z^{(m)} \overline{S}_{zx}^{(n)} \right) dz \right]. \tag{18}$$

The uniform pressure P produced by the piston-like action of the transducer was considered. The integral in the right side, can be proven [7] to be the reciprocal work between Lamb modes *m* and *n*, which is $S_n W_{nn} \delta_{nm}$, using the Kronecker symbol $\delta_{mn} = \begin{cases} 0 \; if \; m \neq n \\ 1 \; if \; m = n \end{cases}$ and $W_{nn}$ is the time averaged energy flux of the mode n. The infinite sum converges rapidly, and $n_{max}$=20 has been proven to be sufficient for an energy balance $\sum_{n=0}^{20} W_{nn} / W_{inc} \cong 1$ with less than 2% error.

## 4. Material properties

Having in view aeronautical applications, the chosen material is aluminum

in the form of a plate of thickness $h$=3mm. In the present work, the material properties have been determined, for existing samples and using the classical ultrasonic techniques of measuring the bulk ultrasonic waves velocities: longitudinal $c_L$ and respectively transversal $c_T$. The time lapse ($\Delta t_L$ and $\Delta t_T$ respectively) between two successive echoes reaching the transducer, which is applied perpendicular on the plate surface, allows for the computation of the two velocities:

$$c_L = \frac{2h}{\Delta t_L} = 6322.4\ m/s;\ \ c_T = \frac{2h}{\Delta t_T} = 3115.3\ m/s\cdot$$

The mass density was determined from an accurate mass determination using a professional scale and the volume from the measured dimensions (*335.03x200.73x3* mm) of the plate, resulting to be $\rho =$ 2681 kg/m$^3$. Using these material data, the Lamé coefficients λ=55.13 GPa and μ=26.01 GPa are obtained (or the Young modulus E=69.7 GPa and the Poisson coefficient ν=0.34).

## 5. Numerical example

The mathematical method presented in section 3 was applied to a plate of aluminum of relevant material constants obtained as presented in the previous section.

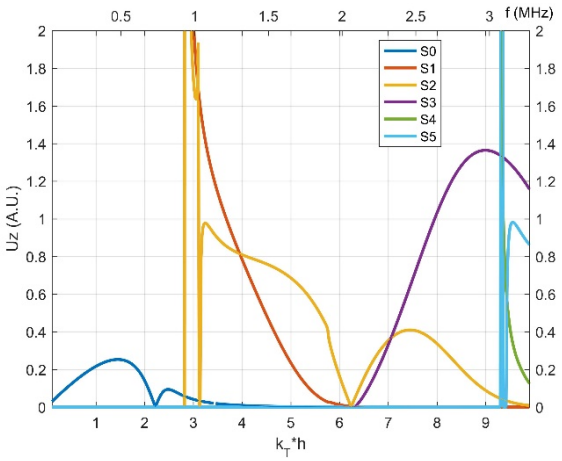


Fig. 4 Modal displacements normal to the plate surface

In order to obtain a wider range of applicable results, the computations and the results are using non-dimensional physical quantities, e.g the non-dimensional

frequency $\Omega = k_T h = \frac{2\pi h}{c_T} f$, but for the tested sample, an upper true frequency scale ($f$ in MHz) is included for an easier comparison of results.

The obtained modal amplitudes for each frequency allow us to determine the normal displacements on the plate surface, for each of the propagating modes over the selected frequency range (Fig. 4). At each non-dimensional / true frequency can be determined also the normal velocities (Fig. 5) for all propagating modes, necessary for comparison with laser velocimeter data.

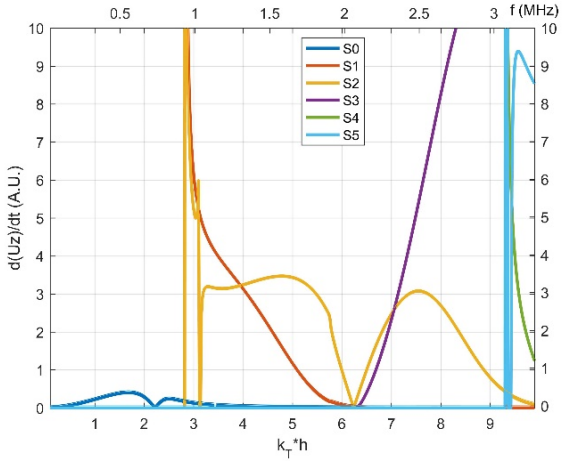


Fig. 5 Modal velocities normal onto the plate surface

For the same longitudinal displacement $U_0$ applied by the harmonic moving piston-transducer at one plate end, the normal displacements and velocities at lower frequencies ($\Omega = k_T.h < 2.8$) corresponding to the $S_0$ mode, are considerably lower than those of the modes $S_1$ and $S_2$ at frequencies just above $\Omega = 3.2$.

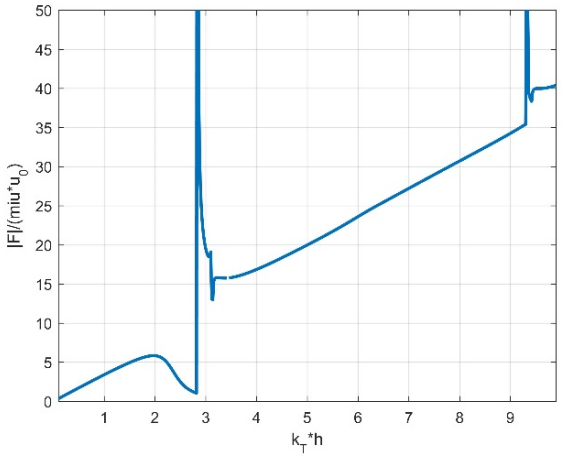


Fig. 6 The force applied at the plate edge vs. frequency for a displacement amplitude $u_0$

The normal displacements and velocity of the mode $S_1$ decreases to vanishing as non-dimensional frequency increases from 3.2 to 6.3. Consequently, it is necessary to compute the axial force of the transducer required to produce the longitudinal displacement $U_0$.

The force required to generate a particular set of modes at a given frequency is obtained as $F/\mu U_0$. The necessary force to be applied at a plate edge for a given edge vibration amplitude is shown on Fig. 6. At the lowest frequencies, below the cutoff frequency of modes $S_1$ and $S_2$, the required force is also low for a given motion amplitude, as it can be expected. An interesting remark is that the force is not increasing monotonically, but a local maximum is reached for a non-dimensional frequency $kt.h = 2$.

The narrow frequency range close to non-dimensional frequency 3 is governed by a rapid variation of wavenumbers in the dispersion curves, reflected by a rapid variation in the required force. This frequency range and all above values are avoided by most specialists. What we suggest in this paper is to consider the higher frequency range $\Omega = 3.2 - 9.2$. In this domain, the required force increases almost linearly with increasing frequency. In other words, for a given force, the ultrasonic modes amplitudes will decrease linearly with increasing frequency. However, as shown on Fig. 5, in the frequency range $k_T.h = 3.2 \ldots 6.3$ the normal velocity of the mode $S_2$ has a relatively constant amplitude, at least below $k_T.h = 5.5$ and could be used for non-destructive applications.

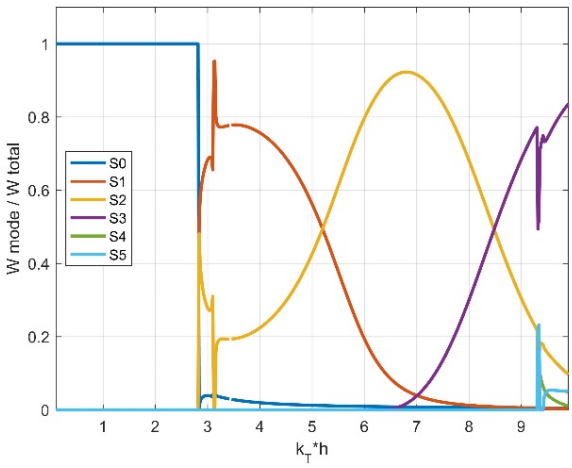


Fig. 7 Relative energy flux of propagating modes vs. frequency (non-dimensional values)

The most important results are represented by the energy flux distribution among the propagating modes as a function of frequency, since the sum of these energy fluxes equal or close to the unit value, represent a validation of the numerical

results. On Fig. 7 are presented the first six propagating modes, from the lowest frequencies, where only S0 mode exists, up to a very high frequency at which all six modes could propagate. As expected, if only the fundamental $S_0$ mode can propagate, the entire energy flux of the ultrasonic transducer applied at the plate edge ($W_{total}$), will be carried by this mode. Even in the transition domain with rapid variations of fluxes, the mathematical model works with high accuracy, but the results are less interesting from a practical point of view. In the emphasized frequency range $\Omega = 3.2 - 9.2$, the incident energy flux is scattered among the propagating modes in a specific manner:

- The fundamental $S_0$ mode is completely absent.
- The $S_1$ mode is energy dominant up to a non-dimensional frequency kt.h = 5.2, but continuously decaying in front of the mode $S_2$ which is reaching a peak of energy flux at kt.h = 6.8.
- Beyond the cutoff frequency kt.h = 6.8, the $S_3$ mode has an increasing energy flux.

## 6. Experimental results

The experiments were conducted in the Laboratory of Structures Integrity Control located in the Department of Mechanics of the University Politehnica of Bucharest. The experimental setup consists of a Polytec laser vibrometer using a OFV-505 sensor head with highest central frequency of $f_{cen}$ = 1 MHz. A Pulser-Receiver is used to generate the ultrasonic pulses at the plate edge, by a GE Krautkramer H1K or H2K ultrasonic transducers of central frequencies 1 MHz and 2 MHz respectively. The overall setup is presented on Fig. 8a depicting the main devices and their connections. The aluminum plate is displaced vertically downwards in steps of 0.075 mm (Fig. 8b,c). The signals shown on the oscilloscope are stored on a USB stick. The ultrasonic signals detected by the Laser vibrometer are recorded with a step of 0.075 mm for a total of 500 steps. A detailed signal processing is done by the double Fourier transform. The time domain is transformed into the frequency domain and the spacing evolution at a fixed time is transformed into wavenumbers. This is done by a proprietary signal processing algorithm developed in GNU Octave scientific programming software [15].

By plotting this frequency-wavenumber results, one can determine the propagating modes in the plate, by a direct comparison to the computed dispersion curves. The first transducer used (H1K) has a design central frequency of 1 MHz. Moreover the Laser vibrometer is configured to work up to 1 MHz. No cut-off filters were used. The results are plotted on Fig. 9a.

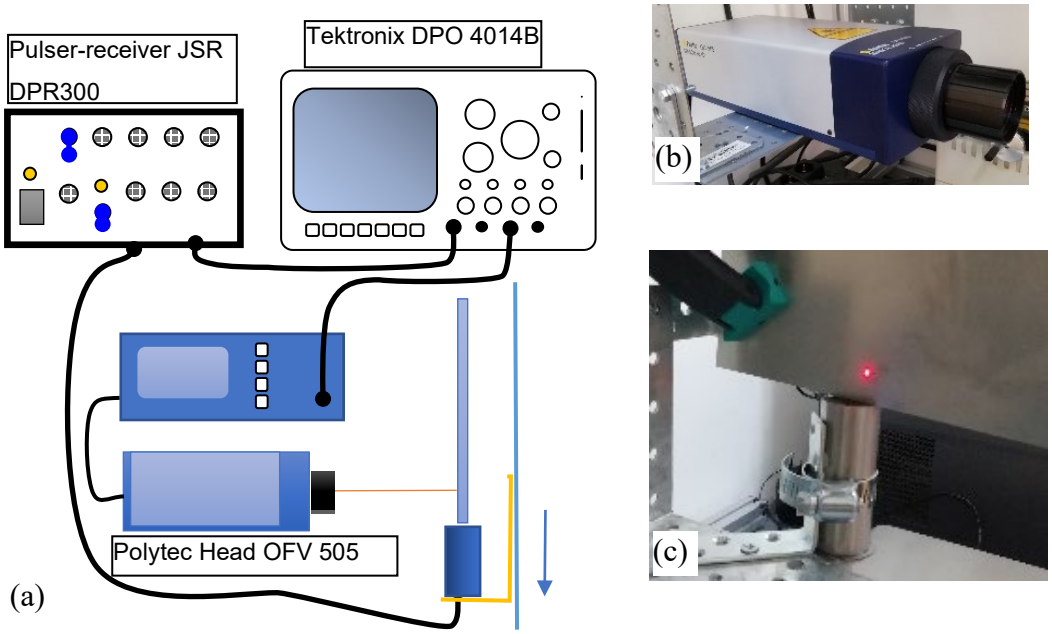


Fig. 8 Experimental setup (a). Laser vibrometer head (b) and aluminum plate on top of the ultrasonic transducer (c) with the laser spot visible

The superposition of the numerically calculated dispersion curves from Fig. 3, shown here as dashed lines, proves to be very good and the Lamb modes can be identified. It is apparent that the highest amplitude is focused on the $S_0$ mode below 1 MHz. Very weak amplitudes are also for the $A_0$, $S_1$ and $S_2$ modes.

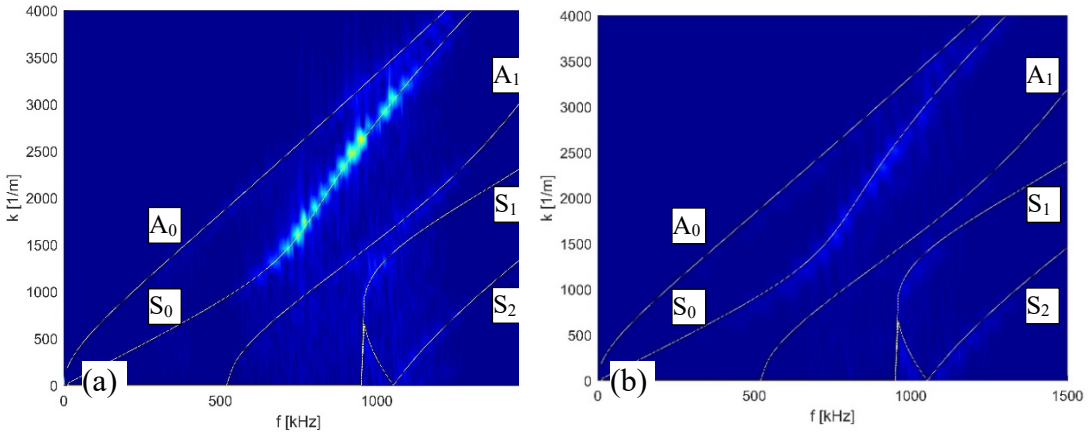


Fig. 9 Experimental dispersion curves, for a transducer of 1 MHz (a) and 2 MHz (b)

The presence of the $A_0$ mode can only be caused by small imperfections in the geometrical symmetry and perpendicularity of the plate edge. Very weak

amplitudes can be seen also for the $S_0$ mode above the frequency of 1 MHz. For this reason, the experiments were resumed with a H2K transducer with a central frequency of 2 MHz. Unfortunately the Laser vibrometer has a weak sensitivity above 1 MHz, so that the results shown on Fig. 9b are confirming this. However, the lighter spots indicate as before, the individual propagating Lamb modes. The $S_0$, $S_1$ and $S_2$ modes are visible even at frequencies higher than 1 MHz.

This result is very important for future development of inspection techniques at non-dimensional frequencies $k_T.h = 3.2 \ldots 5.5$. Even if at these frequencies, the normal force on the plate edge produced by the transducer is several times larger, the advantages of obtaining shorter wavelengths can prove efficient in detecting smaller defects.

## 7. Conclusions

The continuously increasing accuracy requirements for ultrasonic inspections leads to an increase in the frequency of the ultrasonic waves. In aeronautical applications, guided waves are increasingly applied for their rapid coverage of large areas of aluminum panels. However, the complexity of the dispersion curves at these high frequencies, represented a major setback in using high frequencies at which multiple modes can propagate.

In the present paper was used a mathematical and numerical method, developed by one of the authors in previous papers, capable to solve for the full set of complex values of the wavenumbers. These continuous dispersion curves were used in a series development of the applied piston-like displacement field. Using the reciprocity theorem, the amplitudes of each Lamb mode is obtained, for a wide frequency range.

The modal amplitudes, thus obtained have been used to determine the required force of the transducer for a given plate edge harmonic motion. The evolution of this force vs. frequency has proven to be non-monotonic, a fact which was not reported before. The normal displacements and velocities were determined for each propagating mode over a wide range of frequencies.

An even more useful result is the incident energy flux scattering among the propagating modes. In the suggested frequency range for ultrasonic inspection, it is proven that the symmetric Lamb mode $S_2$ is a principal candidate. The best frequency range, recommended in case of using a Laser vibrometer as signal detector, is between $k_T.h = 3.2 \ldots 5.5$, for which the $S_2$ mode provides a constant high normal velocity and a high energy flux.

The original experiments done in one university laboratory have confirmed the theoretical and numerical results, with limitations in the highest measurable frequency. Potential applications in the aeronautical industry are in

the cracks and flaws detection over large aluminum panels, covered by propagating Lamb modes.

## REFERENCES

[1] *H. Lamb*, “On waves in an elastic plate”, *Proceedings of the Royal Society of London. Series A.,* vol. 93, pp. 114-128, 1 March 1917.

[2] *J. Miklowitz*, The Theory of Elastic Waves and Waveguides, I ed., Amsterdam: North Holland, 1978.

[3] *J. D. Achenbach*, The Evaluation of Materials and Structures by Quantitative Ultrasonics, Wien: Springer Verlag, 1993.

[4] *I. A. Viktorov*, Rayleigh and Lamb Waves: Physical Theory and Applications, New York: Springer-Verlag, 1967.

[5] *W. B. Fraser,* "Orthogonality relation for the Rayleigh-Lamb modes of vibration of a plate," *The Journal of the Acoustical Society of America,* vol. 59, no. 1, pp. 215-216, 1976.

[6] J. *E. Murphy and S. A. Chin-Bing*, "Orthogonality relation for Rayleigh - Lamb modes of vibration of an arbitrarily layered elastic plate with and without fluid loading," *J. Acoust. Soc. Am.,* vol. 96, no. 4, pp. 2313-2317, 1994.

[7] *P. J. Torvik*, "Reflection of wave trains in semi-infinite plates," *J. Acoust. Soc. Am.,* vol. 41, p. 346–353, 1967.

[8] *R. D. Gregory and I. Gladwell*, "The reflection of a symmetric Rayleigh-Lamb wave at a fixed or free edge of a plate," *J. Elasticity,* vol. 13, pp. 185-206, 1983.

[9] *J. M. Galan and R. Abascal*, "Numerical simulation of Lamb wave scattering in semi-infinite plates," *Int. J. Numer. Methods Eng.,* vol. 53, p. 1145–1173, 2002.

[10] *J. Galan and R. Abascal*, "Lamb mode conversion at edges. A hybrid boundary element–finite-element solution," *J. Acoust. Soc. Am.,* vol. 117, no. 4, p. 1777–1784, 2005.

[11] *M. Predoi and M. Rousseau*, "Recent results about lamb waves reflection at the free edge of an elastic layer," *Acta Acustica (Stuttgart),* vol. 89, no. 4, 2003.

[12] *M. V. Predoi*, "Properties of non-propagating guided waves in plates," *Romanian Journal of Acoustics and Vibrations,* vol. 1, no. 1, pp. 61-70, 2004.

[13] *E. Le Clezio, M. Predoi, M. Castaings, B. Hosten and M. Rousseau*, "Numerical predictions and experiments on the free-plate edge mode," *Ultrasonics,* vol. 41, no. 1, 2003.

[14] *P. R. Brazier-Smith and J. F. M. Scott*, "On the determination of the roots of dispersion equations by use of winding number integral," *J. Sound Vib. ,* vol. 145, p. 503–510, 1991.

[15] *** GNU OCTAVE, Scientific Programming Language, User Manual, 2021